On the interaction of solutes with grain boundaries

Remi Dingreville, Stéphane Berbenni

SAND2015-10306J

On the interaction of solutes with grain boundaries

Rémi Dingreville[a,*], Stéphane Berbenni[b]

[a]*Sandia National Laboratories, Albuquerque, NM 87185, USA*
[b]*Laboratoire d'Étude des Microstructures et de Mécanique des Matériaux, LEM3, UMR CNRS 7239, Université de Lorraine, Île du Saulcy, 57045 Metz, France*

Abstract

Solute segregation to grain boundaries is considered by modeling solute atoms as misfitting inclusions within a disclination structural unit model describing the grain boundary structure and its intrinsic stress field. The solute distribution around grain boundaries is described through Fermi-Dirac statistics of site occupancy. The susceptibility of hydrogen segregation to symmetric tilt grain boundaries is discussed in terms of the misorientation angle, the defect type characteristics at the grain boundary, temperature, and the prescribed bulk hydrogen fraction of occupied sites. Through this formalism, it is found that hydrogen trapping on grain boundaries clearly correlates with the grain boundary structure (i.e. type of structural unit composing the grain boundary), and the associated grain boundary misorientation. Specifically, for symmetric tilt grain boundaries about the [001] axis, grain boundaries composed of both B and C structural units show a lower segregation susceptibility than other grain boundaries. A direct correlation between the segregation susceptibility and the intrinsic net defect density is provided through the Frank-Bilby formalism. Overall, the present formulation could prove to be a simple and useful model to identify classes of grain boundaries relevant to grain boundary engineering.

Keywords: Grain boundaries, Dislocations, Disclinations, Solubility, Segregation

1. Introduction

Solute-atom segregation to grain boundaries (GBs) and other microstructural line defects such as dislocations substantially affects their fundamental physico-chemical properties, e.g. grain boundary energy [1–3], grain boundary mobility [4–7], and grain boundary cohesion [8–10], which in turn impacts a wide range of material behaviors including strain aging [11–13], intergranular fracture [14, 15], recrystallization [16, 17], and creep [18, 19]. The chemical equilibrium distribution of solutes in a solid determines the interaction between these solutes and defects already existing in a material system and plays a key role in the nature of the subsequent mechanisms governing the behaviors listed above.

*Corresponding author
Email address: rdingre@sandia.gov (Rémi Dingreville)

It has been established, both experimentally [8, 20–22] and theoretically [11, 23–27], that solute equilibrium depends on the intrinsic character of the defect considered and its associated pre-existing stress field. Of particular theoretical interest, Cai et al. [27] recently clarified the formalism of how the equilibrium configuration of solutes should depend on the stress field in an isotropic elastic solid. This formulation models the chemical equilibrium distribution of point defects as non-overlapping spherical inclusions with purely positive dilatational eigenstrain. This formulation excludes the *self-stress* of the inclusions (hydrostatic stress found *inside* the inclusion), but accounts for the *image stresses* introduced to satisfy the boundary conditions in a finite solid. The solute distribution around a given defect d follows Fermi-Dirac statistics on the hydrostatic stress field produced by the defect considered, the stress fields generated by other defects, and stress field generated by external loads. This non-uniform distribution of solutes around a defect d is accompanied by a coherency stress preserving the coherency of the crystal lattice. In an infinite isotropic elastic medium it has been shown [24, 27] that the coherency stress is directly proportional to the local concentration of solutes and the solute distribution throughout the entire solid.

Most of the theoretical treatments concerning the interaction between solute atoms and defects focus on dislocation-type defects [11, 24, 27–32]. For example, Cottrell and Bilby [11, 28, 29] and later work extended by others [24, 27, 31, 32] have examined the equilibrium solute distribution around a single infinitely long straight dislocation. In the case of an edge dislocation, the total depletion of solutes shows a logarithmic dependence beneath the glide plane. Webb [30] extended this theory to the case of dislocation walls or small angle grain boundaries by summing the contributions of an array of individual lattice dislocations as classically defined in dislocation theory [33]. However, dislocation-type analyses are limited to simple representations of low-angle boundaries and are not adequate for large-angle boundaries, low symmetry crystals, very short boundaries of any angle and other types of more complex defects like triple junctions.

Another paradigm which can be used to model more complicated grain boundary structures in terms of linear defects instead constructs grain boundaries using disclinations [34–41]. Disclination-based models are fully equivalent to dislocation models in terms of their stress and strain fields, and are also particularly advantageous for obtaining the mechanical field of a general grain boundary where dislocation cores would overlap as is the case for large angle GBs. Similarly, models of other complex defects such as triple junctions [40] or the structure of zigzag tilt GBs [38] can be constructed using disclinations. Such defects are of particular interest since they constitute stress concentrators within any given microstructure potentially providing additional driving force for solute segregation.

The present analysis, which is based on the formalism suggested by Cai et al. [27], treats solute atoms as misfitting spherical inclusions and considers their interactions with (tilt) grain boundaries (about the [001] axis). The adopted model accounts for the complex structure of grain boundaries through disclination-based models and considers the material as linear, elastic, and isotropic. Hydrogen segregation to grain boundaries is explored for a wide variety of grain boundaries. Of particular interest, correlations between grain boundaries' segregation susceptibility, the grain boundary misorientation and the grain boundary structural character is investigated. The susceptibility to hydrogen segregation of symmetric

tilt grain boundaries is discussed in terms of the misorientation angle and the intrinsic grain boundary defect type characteristics.

The manuscript is thus organized as follows. Section 2 details the construction of grain boundaries using disclination theory and the resulting solute distribution. Section 3 discusses the correlation between solute concentration and the grain boundary defect characteristics. Conclusions are drawn concerning the application of this model in Section 4.

2. Solute distribution around grain boundaries

As mentioned in Section 1, so-called superatomic (mesoscopic) disclination-based models provide a convenient way of representing grain boundary behavior under various loading conditions using linear theory of defects. Wedge disclination dipoles are the basic ingredients of such models [39]. As illustrated in Fig. 1(a), disclinations are linear rotational defects [42] for which, similar to the way dislocations are characterized in continuum mechanics using the Burgers vector, the strength of a disclination is related to an axial pseudo vector $\overrightarrow{\omega}$ (Frank's vector) defining the rotation between two cut surfaces. The elastic fields of straight disclinations in an elastic infinite isotropic medium can be found in analytical form based on the general linear elastic theory of defects [43, 44]. Following deWit [43], the stress field $\sigma^{\triangleright}_{ij}(x,y)$ of a pure wedge disclination located at the origin with a Frank's (pseudo) vector magnitude (or strength) ω (see Fig. 1) is given in a Cartesian coordinate system by:

$$\sigma^{\triangleright}_{xx}(x,y,\omega) = D_0\omega\left(\ln\sqrt{x^2+y^2} + \frac{y^2}{x^2+y^2}\right) = D_0\omega\left(\ln r + \frac{y^2}{r^2}\right) \ , \tag{1}$$

$$\sigma^{\triangleright}_{yy}(x,y,\omega) = D_0\omega\left(\ln\sqrt{x^2+y^2} + \frac{x^2}{x^2+y^2}\right) = D_0\omega\left(\ln r + \frac{x^2}{r^2}\right) \ , \tag{2}$$

$$\sigma^{\triangleright}_{xy}(x,y,\omega) = -D_0\omega\frac{xy}{x^2+y^2} = -D_0\omega\frac{xy}{r^2} \ , \tag{3}$$

$$\sigma^{\triangleright}_{zz}(x,y,\omega) = \nu\left[\sigma^{\triangleright}_{xx}(x,y) + \sigma^{\triangleright}_{yy}(x,y)\right] \ , \tag{4}$$

where $r^2 = x^2+y^2$, μ is the shear modulus, ν is the Poisson's ratio and $D_0 = \dfrac{\mu}{2\pi(1-\nu)}$.

Note that the logarithmic divergence of the long-range stress fields of a wedge disclination implies that disclinations can exist only in a screened state by configuring straight disclinations in dipoles or other multipole configurations. The stress field of such arrangements can be found by superposition of the contributions from individual straight disclinations. As such, the stress field $\sigma^{\bowtie}_{ij}(x,y)$ of a disclination dipole (ω, L) centered at $y=0$ with positive disclination $+\omega$ at $(0,L)$ and negative disclination $-\omega$ at $(0,-L)$ (see Fig. 1(b)) is given by:

$$\sigma^{\bowtie}_{ij}(x,y,\omega,L) = \sigma^{\triangleright}_{ij}(x,y-L,\omega) - \sigma^{\triangleright}_{ij}(x,y+L,\omega) \ . \tag{5}$$

2.1. Construction of grain boundaries using the disclination structural unit model (DSUM)

Originally proposed by Shih and Li [34, 35] and later improved by Gertsman et al. [36], the disclination structural unit model (DSUM) constructs a (non-favored) grain boundary

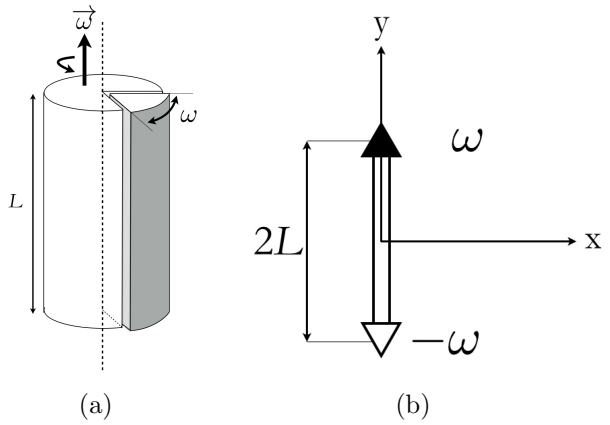

Figure 1: (a) Volterra process in an elastic cylinder for a wedge disclination with Frank vector (rotation pseudo-vector) ω parallel to the line of the defect L. (b) Disclination dipole with a positive disclination $+\omega$ located at $(0, L)$ and a negative disclination $-\omega$ located at $(0, -L)$.

with a misorientation angle θ by decomposing it into a contiguous and alternating sequence of special (favored) m majority and n minority structural units with associated misorientation angles θ_m and θ_n respectively such that $\theta_m < \theta < \theta_n$. Favored boundaries are grain boundaries that have a structure characterized by a repeating sequence of only one type of structural units. As a result the boundary is represented in the form of a complex wall of disclinations combined into dipoles associated with the minority structural units (see Fig. 2(a)). The strength of the disclination dipoles associated with the minority structural unit is equal to $\pm\omega = \pm(\theta_n - \theta_m)$, the arm of the dipoles is fixed and set to L'_n, and the period of the grain boundary is given by $H = (md'_m + nd'_n) = 2(mL'_m + nL'_n)$.

As illustrated in Table 1 [45–47], all symmetric tilt grain boundaries about the [001] axis can be decomposed into primary structural units that are consistent with the four favored [001] symmetric tilt grain boundaries: the A structural unit $\Sigma1$ (1 1 0) / $\theta = 0°$ perfect lattice, the B structural unit $\Sigma5$ (2 1 0) / $\theta = 36.87°$ grain boundary, the C structural unit $\Sigma5$ (3 1 0) / $\theta = 53.13°$ grain boundary, and the D structural unit $\Sigma1$ (1 0 0) / $\theta = 90°$ perfect lattice. Thus, all symmetric tilt grain boundaries about the [001] axis with a misorientation $0° \leq \theta < 36.87°$ are composed of only A and B structural units, all boundaries with a misorientation $36.87° \leq \theta < 53.13°$ are composed of only B and C structural units, and all boundaries with a misorientation $53.11° \leq \theta < 90°$ are composed of only C and D structural units. Additionally due to the geometric distortions of the (favored) elementary structural units composing a given (non-favored) grain boundary (see Fig. 2(b)), the dimensions L'_m and L'_n can be evaluated from the rest length of the structural units L_m and L_n through the geometric relation [48],

$$L'_m = L_m \cos\left(\frac{\theta - \theta_m}{2}\right) \ , \ L'_n = L_n \cos\left(\frac{\theta_n - \theta}{2}\right) \ , \tag{6}$$

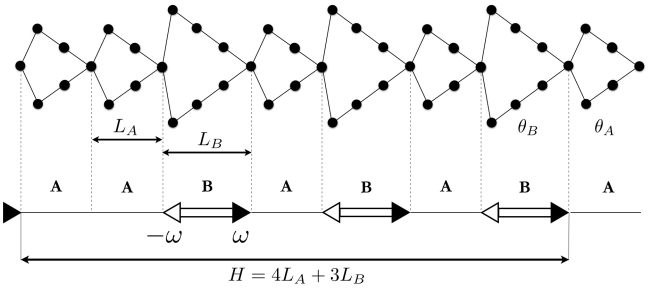

(a)

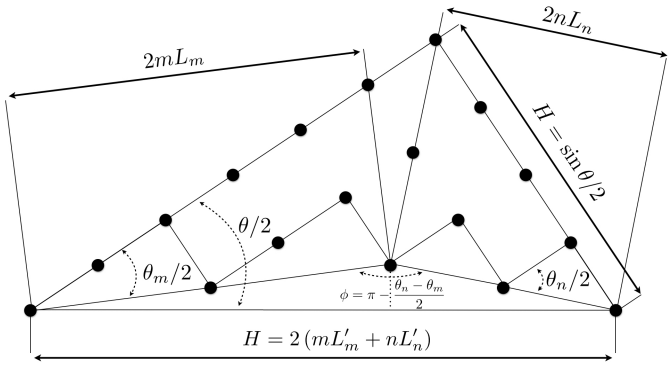

(b)

Figure 2: (a) Disclination Structural Unit Model (DSUM) representation of the [001] $\Sigma = 149/20.02°$ symmetric tilt grain boundary. The filled triangle symbol (►) corresponds to a "positive" disclination, the voided triangle symbol (◅) corresponds to a "negative" disclination. All together they form the disclination dipole associated with the minority structural unit composing the grain boundary. (b) Geometric construct of a symmetric general tilt grain boundary defining the dimensions of the majority and minority structural units. Only the upper part of the grain boundary is shown.

while the average misorientation angle θ is given by,

$$\sin\left(\theta/2\right) = \frac{\left[2mL_m \sin\left(\theta_m\right) + 2nL_n \sin\left(\theta_n\right)\right]}{H} \ . \tag{7}$$

Table 1 and Table 2 summarize the characteristics of the symmetric tilt grain boundaries investigated in this study in the case of nickel (fcc metal).

Following Hurtado et al. [37], the stress field $\sigma_{ij}^{\ddagger,mn}(x,y)$ of a grain boundary composed of m majority and n minority structural units can be mechanistically constructed with an infinite wall of minority disclination dipoles (L'_n, ω) spaced by a distance H such that:

$$\sigma_{ij}^{\ddagger,mn} = \sum_{k=-\infty}^{\infty} \sigma_{ij}^{\bowtie}(x, y, \omega, L'_n + kH) \ . \tag{8}$$

Using series identity formulas [49], equation (8) further reduces to:

$$\frac{1}{2}\left(\sigma_{xx}^{\ddagger,mn} + \sigma_{yy}^{\ddagger,mn}\right) = \frac{1}{2} D_0 \omega \ln \frac{\cosh\alpha - \cos(\beta - \lambda_n)}{\cosh\alpha - \cos(\beta + \lambda_n)} \ , \tag{9}$$

$$\frac{1}{2}\left(\sigma_{xx}^{\ddagger,mn} - \sigma_{yy}^{\ddagger,mn}\right) = \frac{1}{2} D_0 \omega \alpha \left[\frac{\sinh\alpha}{\cosh\alpha - \cos(\beta + \lambda_n)} - \frac{\sinh\alpha}{\cosh\alpha - \cos(\beta - \lambda_n)}\right] \ , \tag{10}$$

$$\sigma_{xy}^{\ddagger,mn} = \frac{1}{2} D_0 \omega \alpha \left[\frac{\sin(\beta + \lambda_n)}{\cosh\alpha - \cos(\beta + \lambda_n)} - \frac{\sin(\beta - \lambda_n)}{\cosh\alpha - \cos(\beta - \lambda_n)}\right] \ , \tag{11}$$

with $\alpha = 2\pi x/H$, $\beta = 2\pi y/H$, and $\lambda_n = 2\pi L'_n/H$.

For example, consider the $\Sigma149$ (10 7 0) / $\theta = 20.02°$ symmetric tilt grain boundary. Its structural decomposition is |AABABAB.AABABAB|, with B being the minority structural unit. The stress field of this grain boundary can be constructed as the superposition of three offsetted infinite walls of disclination dipoles B with an arm length $L'_B = 0.1949$ nm, a strength $\pm\omega = \theta_B - \theta_A = 36.87°$ and a periodicity $H = 2(4L'_A + 3L'_B) = 2.1508$ nm. The first wall is centered at $y = 0$, the second wall is centered at $y = 2(L'_A + L'_B)$, and the third wall is centered at $y = 4(L'_A + L'_B)$. Figures 3 (c)–(f) show contour plots of the $\Sigma149/20.02°$ and $\Sigma181/6.03°$ grain boundaries. It should be noted that the $(\sigma_{xx}^{\ddagger} + \sigma_{yy}^{\ddagger})$ contours are characterized by alternate bands of positive and negative stresses delimited by null contours. Additionally, in the case of the $\Sigma149/20.02°$ grain boundary, the three superimposed infinite walls of disclination dipoles composing the grain boundary can be clearly identified from the presence of alternating stress peaks in the stress contours. Note that for both $\Sigma5$ grain boundaries ($\theta = 36.87°$ and $\theta = 53.13°$), the parameter $\lambda_n = \pi$ such that the DSUM construct predicts that $\sigma_{ij}^{\Sigma5} = 0$.

It is interesting to note that the stress field of a disclination dipole (ω, L) is equivalent to that of a uniform linear distribution of N edge dislocations (see Fig. 4) such that $N = 2L\omega/b$, with b being the Burgers vector [37]. Thus, for low angle tilt grain boundaries ($\theta \leq 15°$) an equivalence to that of equations (9)–(11) can also be represented using an infinite wall of edge dislocations spaced by a distance H with an effective Burgers vector $b_{eq} = Nb = 2L\omega$. The stress field $\sigma_{ij}^{\perp}(x,y)$ of such grain boundaries is classically [33] given by,

$$\frac{1}{2}\left(\sigma_{xx}^{\perp} + \sigma_{yy}^{\perp}\right) = -\sigma_0 \sin 2\pi\frac{y}{H}\left[\cosh 2\pi\frac{x}{H} - \cos 2\pi\frac{y}{H}\right] \ , \tag{12}$$

$$\frac{1}{2}\left(\sigma_{xx}^{\perp} - \sigma_{yy}^{\perp}\right) = -2\pi\sigma_0 \frac{x}{H} \sin 2\pi\frac{y}{H} \sinh 2\pi\frac{x}{H} \ , \tag{13}$$

$$\sigma_{xy}^{\perp} = 2\pi\sigma_0 \frac{x}{H}\left[\cosh 2\pi\frac{x}{H} \cos 2\pi\frac{y}{H} - 1\right] \ , \tag{14}$$

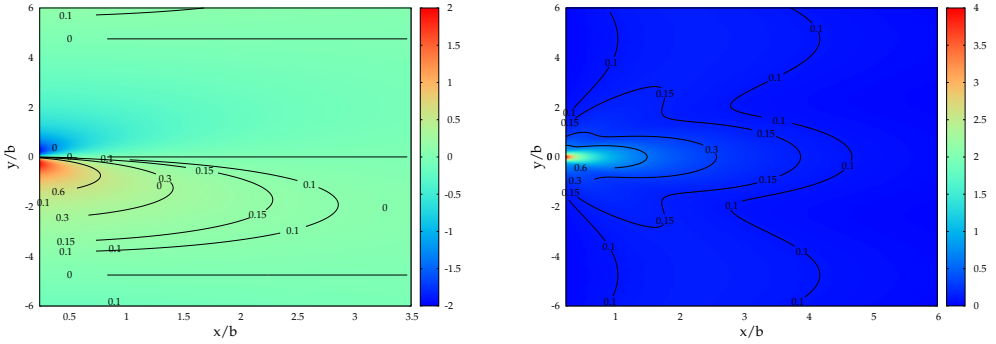

(a) Σ181/6.03° Dislocation wall (b) Σ181/6.03° Dislocation wall

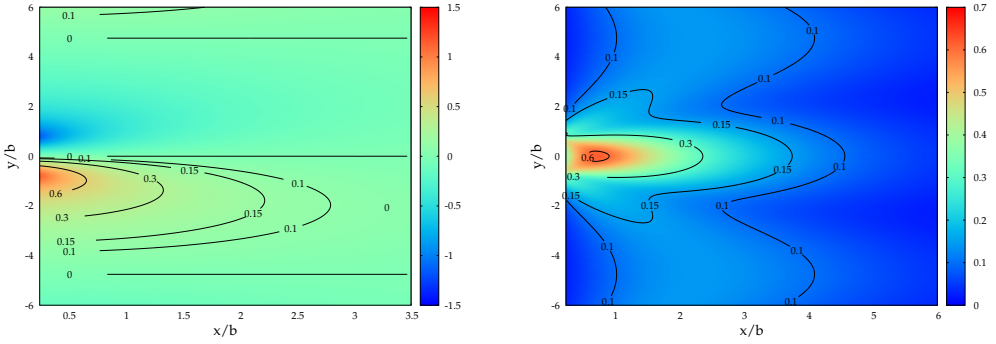

(c) Σ181/6.03° (d) Σ181/6.03°

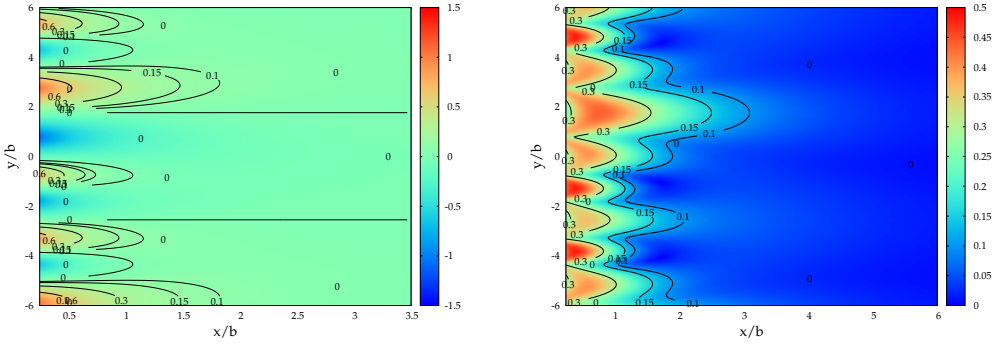

(e) Σ149/20.02° (f) Σ149/20.02°

Figure 3: Contours of the stress field components: (a), (c) and (e) pressure ($(\sigma_{xx}+\sigma_{yy})/D_0$); (b), (d) and (f) stress magnitude ($\sqrt{\left[\sigma_{xy}^2+(\sigma_{xx}-\sigma_{yy})^2/4\right]}/D_0$) for the Σ181/6.03° and Σ149/20.02° grain boundaries respectively. Contours (a) and (b) correspond to the Σ181 tilt grain boundary represented using an infinite edge dislocation wall. Contours (c)–(f) use the DSUM model. Only the contour values for the positive stresses are plotted.

where

$$\sigma_0 = \pi D_0 \frac{b_{eq}}{H} \frac{1}{\left[\cosh\frac{2\pi}{7}\frac{x}{H} - \cos 2\pi\frac{y}{H}\right]^2} \,. \tag{15}$$

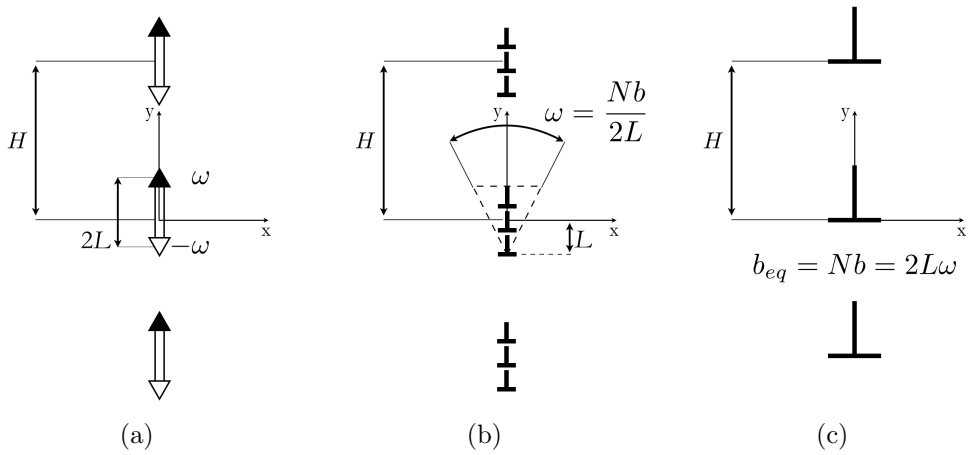

Figure 4: (a) Infinite wall of disclination dipoles (ω, L) spaced by a distance H. (b) Equivalent infinite wall of edge dislocations ($\perp$ symbols) composed of $N = b\omega/2L$ dislocations spaced by a distance H. (c) Equivalent infinite wall of edge dislocations with an effective Burgers vector $b_{eq} = Nb = 2L\omega$.

Figures 3 (a)–(b) show contour plots of the $\Sigma = 181/6.03°$ grain boundary using the dislocation representation. These contours are in agreement with their counterparts using the disclination representation. It should be noted however that the stress magnitude close to the cores of the dislocations are higher and more localized when represented using edge dislocations than in the case of the disclination representation for which core effects are smeared out.

2.2. Solute trapping at grain boundaries

As detailed in Cai et al. [27], the chemo-mechanical equilibrium of interstitial solutes in a homogeneous isotropic elastic medium can be modeled by considering solutes as non-overlapping spherical misfitting inclusions with purely positive dilatational eigenstrain. The derivations consider the energetic contribution and the work done against pre-existing stresses upon the introduction of solutes in the medium of interest.

The solute distribution around a given defect d follows Fermi-Dirac statistics such that the equilibrium fraction of occupied sites $\chi(\mathbf{x})$ in an infinite medium[1] with no pre-existing internal stress sources other than that of the defect considered is given by,

$$\chi(\mathbf{x}) = \frac{1}{1 + \dfrac{1-\chi_0}{\chi_0} \exp\left(-\dfrac{1}{k_B T}\dfrac{1}{3}\sigma_{ii}^d(\mathbf{x})\,\Delta V\right)}\,, \tag{16}$$

where χ_0 is the fraction of occupied sites under zero pre-existing stress, k_B is the Boltzmann constant, T is the absolute temperature, $\sigma_{ii}^d(\mathbf{x})$ is the hydrostatic stress field produced by

[1]Note that in the case of a finite volume the tensile image stress field must be included to satisfy the boundary conditions. Through the image stress, existing inclusions promote the introduction of additional inclusions [27].

the defect considered including the stress fields generated by other defects as well as by external loads, and ΔV is the extra (dilatational) volume of the solute. The volume density c of solutes at equilibrium around d is then given by $c(\mathbf{x}) = \chi(\mathbf{x})\, c_{\max}$, where $c_{\max}$ is the maximum possible volume density of the solutes in the solvent medium. The dependence on the chemical potential μ_i of the solutes in the host medium free of pre-existing defects is implicitly accounted for through the fraction of occupied sites under zero pre-existing stress χ_0 such that,

$$\chi_0 = \frac{1}{1 + \exp\left(\dfrac{1}{k_B T}\left(E_f - \xi\chi_0 - \mu_i\right)\right)} \ , \ \text{with} \ \ \xi = \frac{4\mu\,(1+\nu)}{9\,(1-\nu)}\Delta V^2 c_{\max} \ , \tag{17}$$

where E_f is the energy necessary to insert one solute in an infinite medium and the constant ξ has the dimension of an energy. It should be noted that for high fractions of occupied sites χ_0, the material may undergo a phase transformation (in the case of hydrogen the formation of hydrides for example) that are not accounted for through this model. In the rest of this manuscript, high values of χ_0 are for illustration purposes only.

Let us now consider the equilibrium solute distribution around an infinitely long grain boundary constructed using the disclination structural unit model presented in Section 2.1. When a grain boundary is present in the solid, it produces an internal hydrostatic stress field $\sigma_{ii}^{\ddagger,mn}(\mathbf{x})$ and the solute fraction of occupied sites $\chi^{\ddagger,mn}(\mathbf{x})$ becomes nonuniform, i.e. $\chi^{\ddagger,mn}(\mathbf{x}) = \chi_0 + \Delta\chi(\mathbf{x})$. The field of solute fraction of occupied sites $\chi^{\ddagger,mn}(\mathbf{x})$ in the vicinity of a grain boundary composed of m majority and n minority structural units is given by equation (16) by substituting the defect hydrostatic stress field $\sigma_{ii}^{d}(\mathbf{x})$ by the grain boundary stress field $\sigma_{ii}^{\ddagger,mn}(\mathbf{x})$. The material parameters used in this study corresponding to hydrogen interstitials occupying interstitial sites of FCC Ni are summarized in Table 3.

Figure 5 gives an example of the χ-fields distributed around several grain boundaries for a bulk hydrogen fraction of occupied sites $\chi_0 = 0.1$ and at a temperature $T = 300$K. It can be seen that upon the introduction of the grain boundary in the infinite medium, hydrogen segregates along the grain boundary alternating between hydrogen-free and hydrogen-rich regions corresponding to regions of compressive and tensile hydrostatic pressure respectively. The extent of the segregation along the grain boundary varies depending on the character of the grain boundary and the size of its associated intrinsic elastic fields. For example, as illustrated in the Figs. 5 (c), (d) and for the $\Sigma 29/43.60°$, $\Sigma 29/46.40°$, and $\Sigma 101/78.58°$ grain boundaries respectively, differences can be observed in the spacing between the hydrogen-rich regions and how far these regions extend away from the grain boundaries. Far away from the grain boundary, the equilibrium fraction field $\chi^{\ddagger,mn}(\mathbf{x})$ approaches that of the bulk hydrogen fraction χ_0.

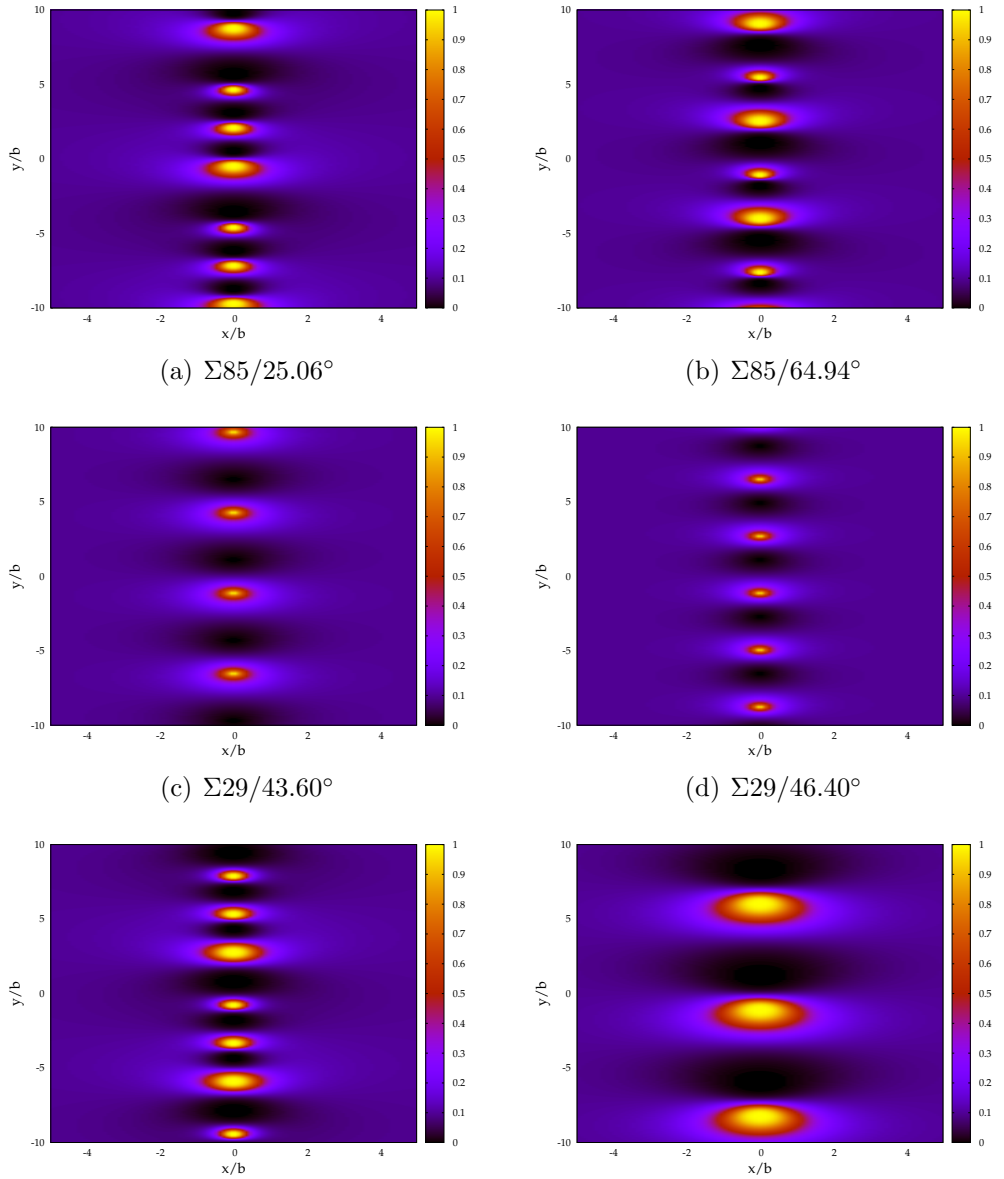

(a) Σ85/25.06° (b) Σ85/64.94°

(c) Σ29/43.60° (d) Σ29/46.40°

(e) Σ149/20.02° (f) Σ101/78.58°

Figure 5: χ-field of solute fraction of occupied sites in the vicinity several grain boundaries: (a) Σ85/25.06°, (b) Σ85/64.94°, (c) Σ29/43.60°, (d) Σ29/46.40°, (e) Σ149/20.02°, and (f) Σ101/78.58° ($\chi_0 = 0.1$ and $T = 300$K).

3. Discussion

3.1. Segregation susceptibility

Through the evaluation of equation (16) giving the field of solute fraction of occupied sites $\chi^{\ddagger,mn}(\mathbf{x})$, the average equilibrium fraction of occupied sites $\overline{\chi}$ trapped in the vicinity S

of a grain boundary (S being a fixed surface running along the grain boundary spanning a length L and going a distance $\pm h/2$ away from the grain boundary line such that $S = hL$. Note that $h/2$ is chosen to be sufficiently large compared to the Burgers vector) is given by,

$$\overline{\chi} = \frac{1}{S} \int_{-h/2}^{h/2} \int_{-L/2}^{L/2} \chi^{\ddagger,mn}(\mathbf{x})\, dxdy \ . \tag{18}$$

This integral has been carried out numerically for $h = 20b$, $L = 100b$ with a resolution of $0.01b$. The segregation susceptibility can be defined $(\overline{\chi} - \chi_0)/\chi_0 = \Delta\chi/\chi_0$ in the vicinity of the grain boundary, with χ_0 being the prescribed bulk hydrogen fraction of occupied sites. In the rest of the discussion, numerical results are presented for symmetric tilt GBs about the [001] axis.

3.2. On the influence of the grain boundary misorientation

First, the segregation susceptibility can be discussed in terms of the grain boundary misorientation θ. Figure 6 illustrates the dependence of the segregation susceptibility $\Delta\chi/\chi_0$ and the solute fraction of occupied sites trapped at the grain boundary as a function of the misorientation θ for a prescribed bulk hydrogen fraction of occupied sites $\chi_0 = 0.01$ at a temperature $T = 300K$. Similar to trends observed for the grain boundary energy as a function of misorientation angles, the grain boundary's solute susceptibility varies smoothly with the misorientation angle, except for cusps corresponding to specific grain boundaries for which the structure changes from one minority structural unit to another. Grain boundaries in the range of $36.87° \leq \theta < 53.13°$ show the smallest ($\Delta\chi/\chi_0 \leq 0.13$) segregation susceptibility while the low angle $\Sigma 41$ (5 4 0) / $\theta = 12.68°$ and the high angle $\Sigma 101$ (10 1 0) / $\theta = 78.58°$ grain boundaries are predicted to be the most susceptible to hydrogen segregation ($\Delta\chi/\chi_0 = 0.57$ and $\Delta\chi/\chi_0 = 0.79$ for the $\Sigma 41$ and $\Sigma 101$ respectively). Additionally, favored grain boundaries associated with local minima (cusps) are predicted to be less susceptible to segregation than neighboring grain boundaries. Thus, the three branches observed in Fig. 6 correspond to misorientation angles of $0° \leq \theta < 36.87°$ composed of only A and B structural units, to misorientation angles $36.87° \leq \theta < 53.13°$ composed of only B and C structural units, and to misorientation angles $53.13° \leq \theta < 90°$ composed of only C and D structural units respectively.

3.3. On the effect of the grain boundary structure

As illustrated by the three branches observed in Fig. 6, segregation susceptibility can also be discussed in terms of the structural units composing the grain boundaries. As highlighted by the symbols, Fig. 6 illustrates the correlation between the grain boundary structure, its misorientation and the amount of solute fraction trapped at the grain boundary (i.e. segregation susceptibility). Figure 7 represents the same data as Fig. 6 but expressed in terms of the characteristic length d'_n of the minority structural unit composing the grain boundary according to the DSUM construct. It is interesting to note that the segregation susceptibility variability is impacted by both the minority structural unit and the associated misorientation angle. For example all the grain boundaries composed of the D structural

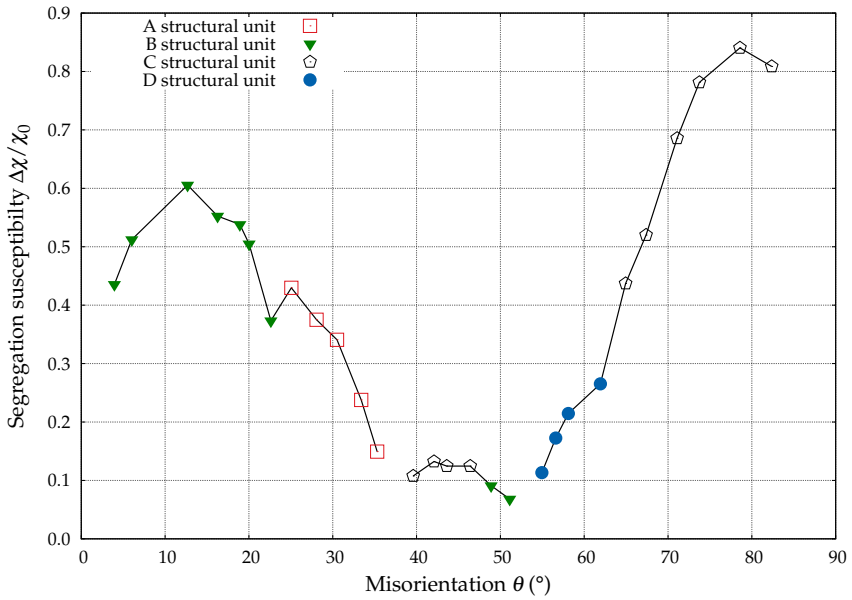

Figure 6: Segregation susceptibility of hydrogen in nickel around symmetric tilt GBs about the [001] axis for a bulk hydrogen fraction $\chi_0 = 0.01$ at $T = 300$K.

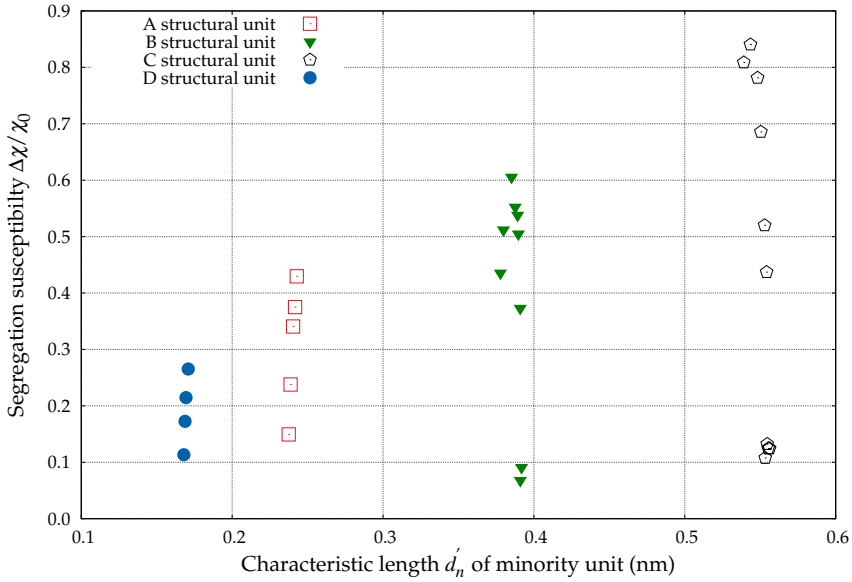

Figure 7: Segregation susceptibility of hydrogen in nickel around symmetric tilt GBs about the [001] axis as a function of the characteristic length d_n' of the minority structural unit composing the GB ($\chi_0 = 0.01$ and $T = 300$K).

unit ($54.95° \leq \theta \leq 61.93°$) show little variation in the segregation susceptibility ($0.1 \leq \Delta\chi/\chi_0 \leq 0.25$) as opposed to grain boundaries composed of the C structural unit ($64.94° \leq$

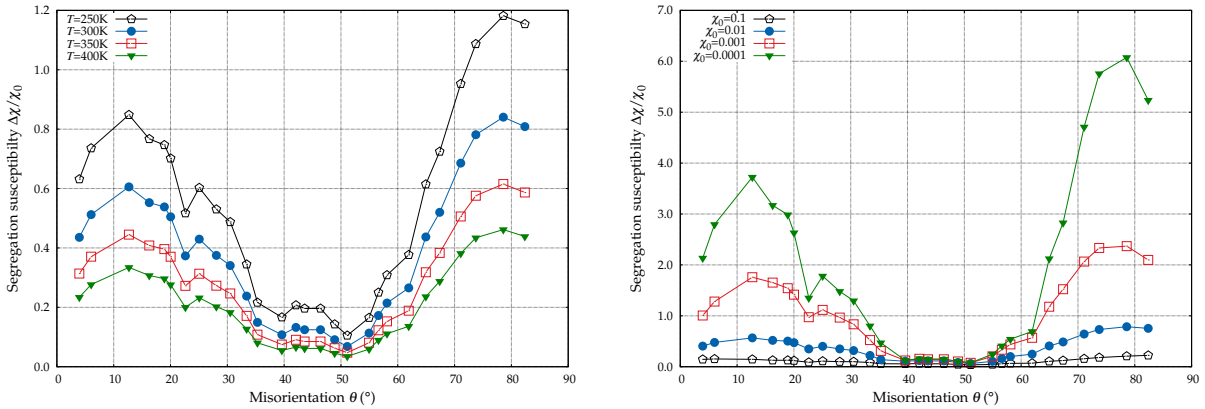

(a) (b)

Figure 8: Segregation susceptibility of hydrogen in nickel around symmetric tilt GBs about the [001] axis: (a) as a function of the temperature for a bulk hydrogen fraction $\chi_0 = 0.01$ and, (b) as a function of the bulk hydrogen fraction χ_0 at $T = 300$K.

$\theta \leq 82.37°$) which show a much larger variation ($0.1 \leq \Delta\chi/\chi_0 \leq 0.8$). The variability in grain boundaries' segregation susceptibility is clearly correlated to the characteristic length (and therefore type) of the minority structural unit. Grain boundaries with the smallest characteristic length (D structural unit) shows the smallest variability (with a variance of 0.003), while grain boundaries with the biggest characteristic length (C structural unit) experience the largest variability (with a variance of 0.082). This is related to the free volume (effectively) available for hydrogen segregation at the grain boundary. These observations are consistent with experimental characterizations [51] which identified a category of "special" grain boundaries as preferential areas for hydrogen segregation.

3.4. On the effect of the temperature and bulk hydrogen fraction

In equation (16), the amount of hydrogen trapped at grain boundary shows a non-linear dependence on the prescribed bulk hydrogen content and an Arrhenius-type dependence on the temperature. Figure 8(a) shows the effect of temperature on the segregation susceptibility as a function of GB misorientation for temperatures ranging from 250K to 400K, while Fig. 8(b) shows the effect of the prescribed bulk hydrogen fraction χ_0 on the segregation susceptibility as a function of GB misorientation for χ_0 ranging from 0.0001 to 0.1 (as mentioned earlier in Section 2.2 high values of χ_0 are for illustration purposes). For all misorientations, the larger χ_0, the lower the segregation susceptibility, while the opposite trend is observed in terms of the temperature. These sensitivities on the grain boundaries' segregation susceptibility remain less pronounced for grain boundaries with misorientations in the range of $36.87° \leq \theta < 53.13°$ corresponding to symmetric tilt grain boundaries of only B and C structural units. These observations correlate with the points made in the previous subsections.

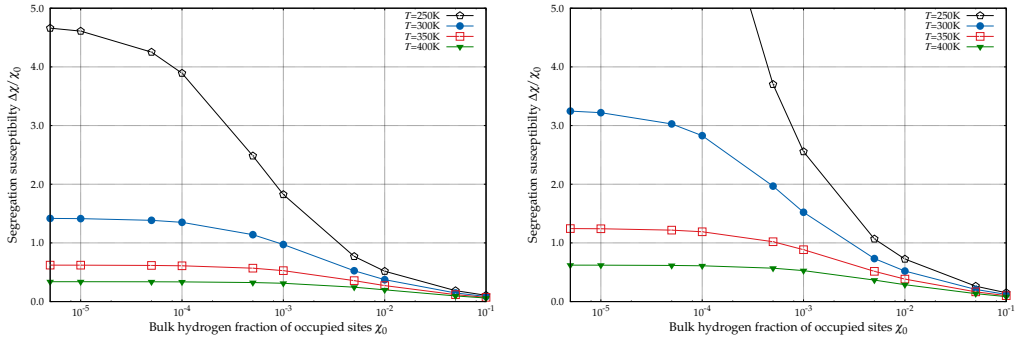

(a) Σ13/22.62° (B structural unit)

(b) Σ13/67.38° (C structural unit)

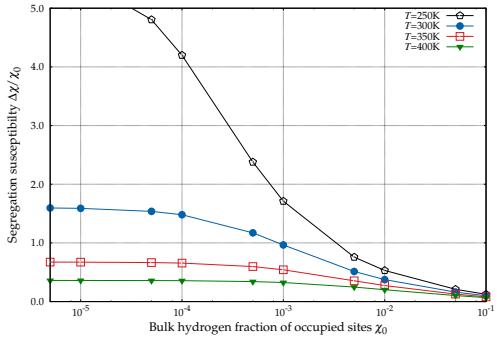

(c) Σ17/28.07° (A structural unit)

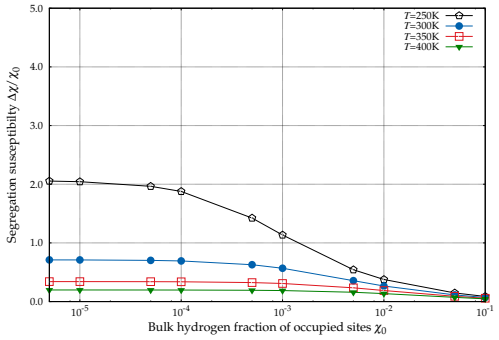

(d) Σ17/61.93° (D structural unit)

Figure 9: Segregation susceptibility of hydrogen in nickel around for the (a) Σ13/22.62° (b) Σ13/67.38° (c) Σ17/28.07° and (d) Σ17/61.93°.

Based on these observations, the segregation susceptibility of particular grain boundaries, namely Σ13 / $\theta = 22.62°$ (B structural unit), Σ13 / $\theta = 67.38°$ (C structural unit), Σ17 / $\theta = 28.07°$ (A structural unit) and Σ17 / $\theta = 61.93°$ respectively, are compared in Fig. 9. This figure emphasizes the non-linear evolution of the grain boundary segregation susceptibility as a function of the bulk hydrogen fraction of occupied sites χ_0 for temperatures ranging from 250K to 400K. As observed previously, the C structural unit grain boundary (see Fig. 9(b)) is the most sensitive to a modification of χ_0. In contrast, the D structural unit grain boundary (see Fig. 9(d)) is much less sensitive to χ_0 than the other structural unit grain boundaries. The general trends shown in Fig. 8 and Fig. 9 are consistent with the observations made by Wolfer and Baskes [24] (see Fig. 2 and Fig. 4 in [24]) who used a model based on bulk dislocation densities. In the present model, for a given material, the segregation susceptibility is not only dependent on the prescribed bulk hydrogen fraction and temperature but also on the grain boundary character. Thus, for polycrystalline materials, the present model sheds light on the complexity and variability in the segregation susceptibility.

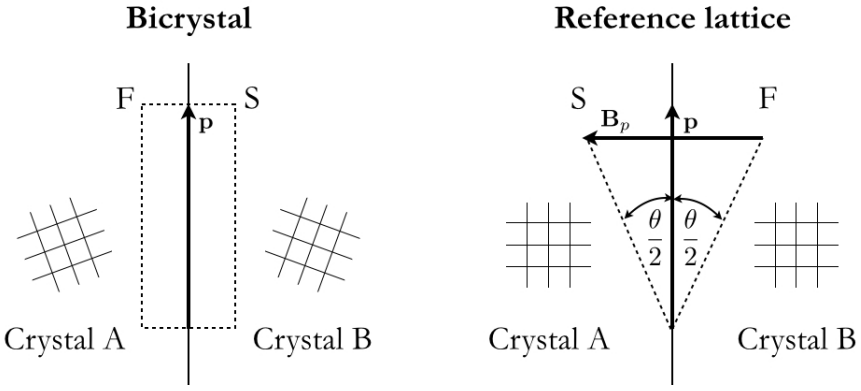

Figure 10: Illustration of the Frank-Bilby formalism for a symmetric tilt grain boundary.

3.5. Correlations with the Frank-Bilby formalism

The results presented in subsections 3.2–3.4 can be put into perspective with respect to the intrinsic net defects density in the sense of the Frank-Bilby formalism. The Frank-Bilby equation [29, 52] is a widely used approach to determine the intrinsic dislocation content of a general boundary (as opposed to extrinsic dislocations which are lattice dislocations interacting with GBs). Within this formalism, based on a Burgers circuit construction, the net Burgers vector $\mathbf{B}_p$ of all interfacial dislocations crossing any vector $\mathbf{p}$ in the interface (i.e. closure failure in the perfect reference lattice) is given by:

$$\mathbf{B}_p = \left(\mathbf{S}_A^{-1} - \mathbf{S}_B^{-1}\right) \cdot \mathbf{p} \ , \tag{19}$$

where $\mathbf{p}$ is the grain boundary period vector, and $\mathbf{S}_A$ and $\mathbf{S}_B$ are lattice deformations (including both rotation and elastic deformation) converting the reference lattice, from which the bicrystal is created, into reference lattices A and B [45]. In other words, $\mathbf{B}_p$ is the resultant Burgers vector of the primary dislocations pierced by the boundary period vector $\mathbf{p}$. In the case of a grain boundary where the two adjoining lattices are related by a misorientation angle only, and taking the median (perfect crystal) lattice as the reference lattice (for primary dislocations), this equation reduces to Frank's formula [45, 53].

For the [001] symmetric tilt grain boundaries considered in this study, the misorientation angle θ is defined in the range $0° < \theta < 90°$ due to the four-fold symmetry around the tilt axis. Following other recent studies on [001] symmetric tilt grain boundaries [54–57], two main Frank-Bilby Burgers vectors (corresponding to two mappings for the Burgers circuit with the "FS (Finish-Start)" right-handed convention) are considered among the multiplicity of solutions of the Frank-Bilby equation. The first possibility (hereafter denoted as "mode I") leads to a net Burgers vector $\mathbf{B}_p$ being parallel to the [100] direction of the reference lattice and the second possibility (hereafter denoted as "mode II") lies in $\mathbf{B}_p$ being parallel to $[\bar{1}\bar{1}0]$ in the reference lattice. Both are dictated by primary Burgers vectors of the resolved discrete distribution of single lattice dislocations for [001] symmetric tilt low-angle grain boundaries close to $\theta = 0°$, i.e. for a Burgers vector $\mathbf{b}$ =a[100], and $\theta = 90°$, i.e. for a

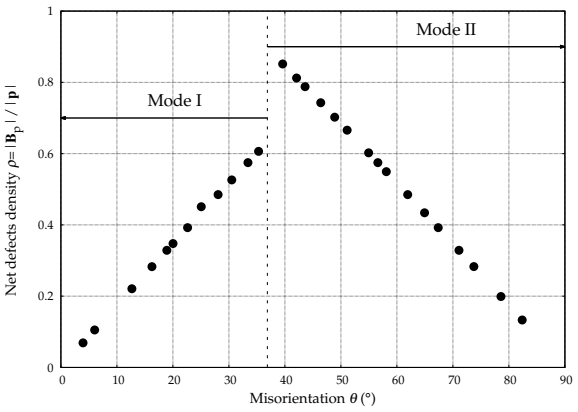

(a)

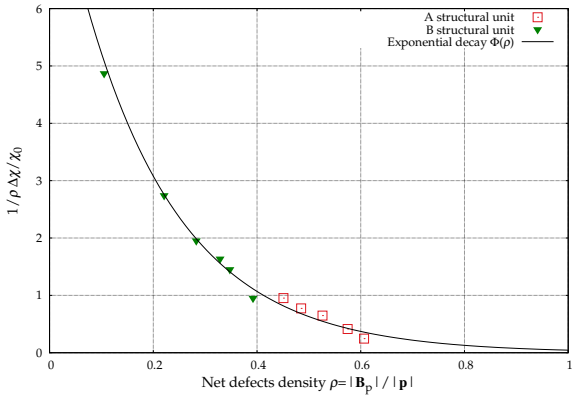

(b) "Mode I"

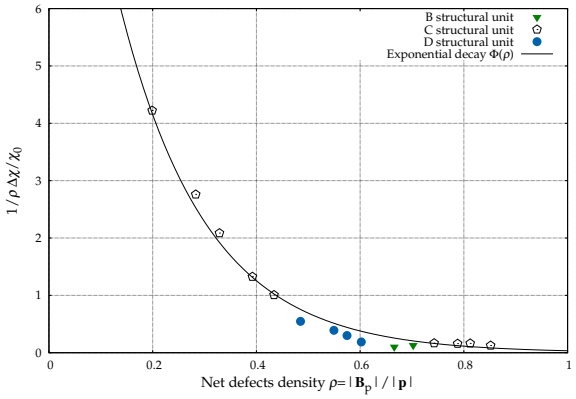

(c) "Mode II"

Figure 11: Equivalence with the Frank-Bilby formalism: (a) Intrinsic net defect density ρ as a function of the misorientation angle θ and, (b) and (c) dependence of $1/\rho\Delta\chi/\chi_0$ as a function of the intrinsic net defect density for various structural units ($\chi_0 = 0.01$ and $T = 300$K) for "mode I" and "mode II" respectively.

Burgers vector $\mathbf{b}$ =a/2$[\bar{1}\bar{1}0]$ (with a being the lattice constant). As reported elsewhere [57], the transition in the interfacial Burgers vector direction (i.e. the transition from $\mathbf{B}_p$ along [100] to $\mathbf{B}_p$ along $[\bar{1}\bar{1}0]$) between "mode I" and "mode II" takes place for the $\Sigma5$ ($\theta = 36.87°$) grain boundary (i.e. the one with a single B structural unit). This particular grain boundary corresponds to a cusp in the grain boundary energy vs. misorientation profile. For both net Burgers vector directions, the intrinsic net grain boundary dislocation density ρ (i.e. net defect representing the initial boundary structure) is given for each boundary in the whole misorientation range around a certain rotation axis by [33, 53, 57]:

$$\rho = \frac{|\mathbf{B}_p|}{|\mathbf{p}|} = 2\sin\left(\frac{\theta}{2}\right) \ . \tag{20}$$

Figure 11 details the equivalence between the DSUM-based model and the Frank-Bilby formalism for the two possible Burgers circuits ("mode I" and "mode II") for $\chi_0 = 0.01$ at

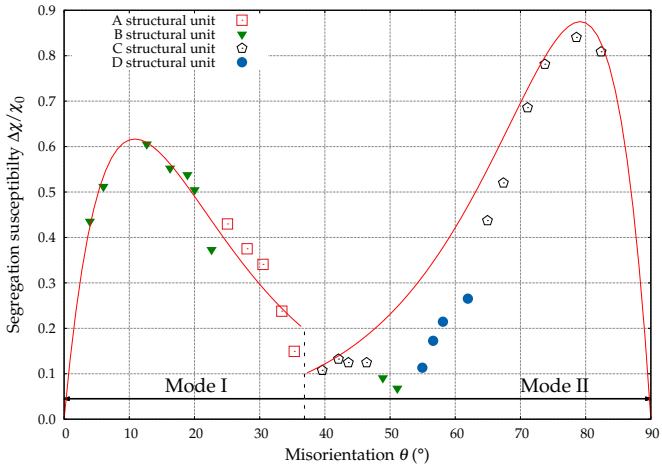

Figure 12: Segregation susceptibility of hydrogen in nickel around symmetric tilt GBs about the [001] axis for a bulk hydrogen fraction $\chi_0 = 0.01$ at $T = 300$K with the susceptibility profile obtained through equation (22).

$T = 300$K. Figures 11 (b) and (c) illustrate the nonlinear dependence of the segregation susceptibility as a function of the intrinsic net defect ρ corresponding to an exponential decay function $\Phi(\rho)$ such that,

$$\frac{\Delta\chi}{\chi_0} = \rho\Phi_i(\rho) = \rho N_i \exp\left(-\lambda_i\left[\rho - \rho_i\right]\right) \ , \tag{21}$$

where the parameters ($N_I = 6.74$, $\lambda_I = 5.29$, $\rho_I = 0.05$) for "mode I" ($i = I$) and ($N_{II} = 6.47$, $\lambda_{II} = 5.97$, $\rho_{II} = 0.12$) for "mode II" ($i = II$) have been fitted through a nonlinear least-squares (NLLS) Marquardt-Levenberg algorithm for both modes. The grain boundary segregation susceptibility follows the same nonlinear trend $\rho\Phi(\rho)$ in equation (21) for both modes as a function of the net defect density for all minority structural units.

Thus, through the Frank-Bilby formalism, grain boundary segregation susceptibility in equation (21) can be explicitly described as a function of the grain boundary misorientation for the two selected modes:

$$\frac{\Delta\chi}{\chi_0}(\theta) = \begin{cases} 2\sin\left(\dfrac{\theta}{2}\right)\Phi_I\left(2\sin\left(\dfrac{\theta}{2}\right)\right) & \text{for} \quad \theta < 36.87^\circ \quad (\text{“mode I”}) \ , \\ 2\sin\left(\dfrac{90^\circ-\theta}{2}\right)\Phi_{II}\left(2\sin\left(\dfrac{90^\circ-\theta}{2}\right)\right) & \text{for} \quad \theta > 36.87^\circ \quad (\text{“mode II”}) \ . \end{cases} \tag{22}$$

As seen in Fig. 12, the relation between the grain boundary segregation susceptibility and the misorientation is adequately represented by equation (22) (red line). Finally the choice of the transition between the Burgers circuit was motivated by atomistic simulation performed at 0K [57] but it should be noted that this transition may be temperature dependent.

4. Conclusion

In this work, a continuum linear defect mechanics model is used to study solute segregation to grain boundaries and the associated segregation susceptibility as a function of the grain boundary character. The two ingredients composing this analysis are based on modeling (i) solute atoms as misfitting inclusions with purely positive dilatational eigenstrain and (ii) grain boundaries using a mesoscopic disclination-based model (e.g. DSUM). Upon the construction of the grain boundary through the DSUM, hydrogen segregation is predicted along the grain boundary by alternating hydrogen-free and hydrogen-rich regions corresponding to compressive and tensile hydrostatic pressure fields, respectively. The extent of the segregation domain along the grain boundary varies depending on the character of the grain boundary and the size of its associated intrinsic elastic fields.

Through this model, a direct correlation between the segregation susceptibility, the grain boundary structural character and the associated misorientation is established. Specifically, in the case of symmetric tilt grain boundaries about the [001] axis, the present model predicts that grain boundaries composed of both B and C structural units (i.e. for a misorientation angle ranging from $36.87^\circ \leq \theta < 53.13^\circ$) show a lower segregation susceptibility than other grain boundaries. Through an analogy with the Frank-Bilby formalism the nonlinear dependence of the segregation susceptibility as a function of the intrinsic net defect ρ is obtained and an explicit expression of the grain boundary susceptibility as a function of the misorientation is derived.

Obviously, the significance of this model extends beyond the calculations of segregation profiles for a specific class of grain boundaries. It provides a simple methodology capable of ascertaining segregation susceptibility over a wide range of grain boundary characters typical of those observed in polycrystalline materials and identifies classes of grain boundaries relevant to grain boundary engineering. Such simplistic continuum theoretical tool can be used to orient specific experiments or corresponding atomistic simulations. The results highlighted in this manuscript will be put in perspective with complementary atomistic simulations in a follow-up study by the authors.

Finally, while the focus of this manuscript was on segregation of hydrogen at grain boundaries, the non-uniform distribution $\chi^{\ddagger,mn}(\mathbf{x})$ of solutes around grain boundaries in equation (16) is accompanied by a coherency stress σ^c preserving the coherency of the crystal lattice. An extension of the present formulation to study the change in elastic fields is beyond the scope of this manuscript but will be presented in detail in a subsequent study by the authors.

Acknowledgment

Supported by the Laboratory Directed Research and Development program at Sandia National Laboratories, a multi-program laboratory managed and operated by Sandia Corporation, a wholly owned subsidiary of Lockheed Martin Corporation, for the U.S. Department of Energy's National Nuclear Security Administration under contract DE–AC04–94AL85000. S.B. would also like to thank the support of the French government through the National

Research Agency (ANR) under the program “Investment in the future” (Labex DAMAS referenced as ANR–11–LABX–0008–01). R.D. would like to thank Labex DAMAS and the Laboratoire d’Étude des Microstructures et de Mécanique des Matériaux (LEM3) for hosting him during the summer of 2015 to complete this work.

References

[1] D. Gupta, Influence of solute segregation on grain-boundary energy and self-diffusion, Metallurgical Transactions A 8 (1977) 1431–1438.

[2] H. Sautter, H. Gleiter, G. Bäro, The effect of solute atoms on the energy and structure of grain boundaries, Acta Metallurgica 25 (1977) 467–473.

[3] R. Kirchheim, Reducing grain boundary, dislocation line and vacancy formation energies by solute segregation. I. Theoretical background, Acta Materialia 55 (2007) 5129–5138.

[4] G. Schoeck, Moving dislocations and solute atoms, Physical Review 102 (1956) 1458.

[5] J. Bernardini, P. Gas, E. D. Hondros, M. P. Seah, The role of solute segregation in grain boundary diffusion, Proceedings of the Royal Society of London. A. Mathematical and Physical Sciences 379 (1982) 159–178.

[6] G. Gottstein, L. S. Shvindlerman, Grain boundary migration in metals: thermodynamics, kinetics, applications, CRC press, 1999.

[7] N. Ma, S. A. Dregia, Y. Wang, Solute segregation transition and drag force on grain boundaries, Acta Materialia 51 (2003) 3687–3700.

[8] M. P. Seah, Segregation and the strength of grain boundaries, Proceedings of the Royal Society of London. A. Mathematical and Physical Sciences 349 (1976) 535–554.

[9] J. P. Stark, H. L. Marcus, The influence of segregation on grain boundary cohesion, Metallurgical Transactions A 8 (1977) 1423–1429.

[10] G. S. Painter, F. W. Averill, Effects of segregation on grain-boundary cohesion: A density-functional cluster model of boron and sulfur in nickel, Physical Review Letters 58 (1987) 234.

[11] A. H. Cottrell, B. A. Bilby, Dislocation theory of yielding and strain ageing of iron, Proceedings of the Physical Society. Section A 62 (1949) 49.

[12] T. Mura, E. A. Lautenschlager, J. O. Brittain, Segregation of solute atoms during strain aging, Acta Metallurgica 9 (1961) 453–458.

[13] J. D. Baird, The effects of strain-ageing due to interstitial solutes on the mechanical properties of metals, Metallurgical Reviews 16 (1971) 1–18.

[14] R. M. Latanision, H. Opperhauser, The intergranular embrittlement of nickel by hydrogen: the effect of grain boundary segregation, Metallurgical Transactions 5 (1974) 483–492.

[15] A. Kumar, B. L. Eyre, Grain boundary segregation and intergranular fracture in molybdenum, Proceedings of the Royal Society of London. A. Mathematical and Physical Sciences 370 (1980) 431–458.

[16] M. B. Kasen, Solute segregation and boundary structural change during grain growth, Acta Metallurgica 31 (1983) 489–497.

[17] R. Kirchheim, Grain coarsening inhibited by solute segregation, Acta Materialia 50 (2002) 413–419.

[18] F. Wakai, T. Nagano, T. Iga, Hardening in creep of alumina by zirconium segregation at the grain boundary, Journal of the American Ceramic Society 80 (1997) 2361–2366.

[19] J. Cho, C. M. Wang, H. M. Chan, J. M. Rickman, M. P. Harmer, Role of segregating dopants on the improved creep resistance of aluminum oxide, Acta Materialia 47 (1999) 4197–4207.

[20] M. P. Seah, E. D. Hondros, Grain boundary segregation, Proceedings of the Royal Society of London. A. Mathematical and Physical Sciences 335 (1973) 191–212.

[21] M. Aoki, Y.-M. Chiang, I. Kosacki, H. Lee, L .and Tuller, Y. Liu, Solute segregation and grain-boundary impedance in high-purity stabilized zirconia, Journal of the American Ceramic Society 79 (1996) 1169–1180.

[22] R. Kirchheim, Reducing grain boundary, dislocation line and vacancy formation energies by solute segregation: II. Experimental evidence and consequences, Acta Materialia 55 (2007) 5139–5148.

[23] F. C. Larché, J. W. Cahn, The effect of self-stress on diffusion in solids, Acta Metallurgica 30 (1982) 1835–1845.

[24] W. G. Wolfer, M. I. Baskes, Interstitial solute trapping by edge dislocations, Acta Metallurgica 33 (1985) 2005–2011.

[25] P. Sofronis, H. K. Birnbaum, Mechanics of the hydrogen-dislocation-impurity interactions–I. Increasing shear modulus, Journal of the Mechanics and Physics of Solids 43 (1995) 49–90.

[26] D. R. Trinkle, C. Woodward, The chemistry of deformation: How solutes soften pure metals, Science 310 (2005) 1665–1667.
[27] W. Cai, R. B. Sills, D. M. Barnett, W. D. Nix, Modeling a distribution of point defects as misfitting inclusions in stressed solids, Journal of the Mechanics and Physics of Solids 66 (2014) 154–171.
[28] A. H. Cottrell, Effect of solute atoms on the behavior of dislocations, in: Report of a Conference on Strength of Solids, 1948, pp. 30–36.
[29] B. A. Bilby, On the interactions of dislocations and solute atoms, Proceedings of the Physical Society. Section A 63 (1950) 191.
[30] W. W. Webb, The interaction of solutes with dislocation walls, Acta Metallurgica 5 (1957) 89–96.
[31] D. M. Barnett, W. C. Oliver, W. D. Nix, The binding force between an edge dislocation and a Fermi-Dirac solute atmosphere, Acta Metallurgica 30 (1982) 673–678.
[32] D. M. Barnett, G. Wong, W. D. Nix, The binding force between a Peierls-Nabarro edge dislocation and a Fermi-Dirac solute atmosphere, Acta Metallurgica 30 (1982) 2035–2041.
[33] J. P. Hirth, J. Lothe, Theory of Dislocations, Second Edition, John Wiley & Sons, Inc., NewYork, NY, 1982.
[34] J. C. M. Li, Disclination model of high angle grain boundaries, Surface Science 31 (1972) 12–26.
[35] K. K. Shih, J. C. M. Li, Energy of grain boundaries between cusp misorientations, Surface Science 50 (1975) 109–124.
[36] V. Y. Gertsman, A. A. Nazarov, A. E. Romanov, R. Z. Valiev, V. I. Vladimirov, Disclination-structural unit model of grain boundaries, Philosophical Magazine A 59 (1989) 1113–1118.
[37] J. A. Hurtado, B. R. Elliott, H. M. Shodja, D. V. Gorelikov, C. E. Campbell, H. E. Lippard, T. C. Isabell, J. Weertman, Disclination grain boundary model with plastic deformation by dislocations, Materials Science and Engineering: A 190 (1995) 1–7.
[38] A. A. Nazarov, O. A. Shenderova, D. W. Brenner, On the disclination-structural unit model of grain boundaries, Materials Science and Engineering: A 281 (2000) 148–155.
[39] A. E. Romanov, A. L. Kolesnikova, Application of disclination concept to solid structures, Progress in Materials Science 54 (2009) 740–769.
[40] M. Upadhyay, L. Capolungo, V. Taupin, C. Fressengeas, Grain boundary and triple junction energies in crystalline media: a disclination based approach, International Journal of Solids and Structures 48 (2011) 3176–3193.
[41] C. Fressengeas, V. Taupin, L. Capolungo, Continuous modeling of the structure of symmetric tilt boundaries, International Journal of Solids and Structures 51 (2014) 1434–1441.
[42] V. Volterra, Sur l'équilibre des corps élastiques multiplement connexes, in: Annales scientifiques de l'École Normale Supérieure, Paris, volume 24, Société mathématique de France, 1907, pp. 401–517.
[43] R. deWit, Theory of disclinations: IV. Straight disclinations, Journal of Research of the National Bureau of Standards, Section A: Physics and Chemistry 77A (1973) 607–658.
[44] T. Mura, Micromechanics of defects in solids, volume 3, Kluwer Academic Publishers, Dordrecht, The Netherlands, 1987.
[45] A. P. Sutton, V. Vitek, On the structure of tilt grain boundaries in cubic metals I. Symmetrical tilt boundaries, Philosophical Transactions of the Royal Society of London A: Mathematical, Physical and Engineering Sciences 309 (1983) 1–36.
[46] G.-J. Wang, V. Vitek, Relationships between grain boundary structure and energy, Acta Metallurgica 34 (1986) 951–960.
[47] P. R. M. van Beers, Multiscale modelling of grain boundary plasticity, Ph.D. thesis, Technische Universiteit Eindhoven, Eindhoven, 2015.
[48] A. A. Nazarov, A. E. Romanov, On the average misorientation angle of general tilt boundaries, Philosophical Magazine Letters 60 (1989) 187–193.
[49] I. S. Gradshteyn, I. M. Ryzhik, Table of Integrals, Series and Products, Academic Press, New York, 2000.
[50] G. J. Thomas, W. D. Drotning, Hydrogen induced lattice expansion in nickel, Metallurgical Transactions A 14 (1983) 1545–1548.

[51] A. Oudriss, J. Creus, J. Bouhattate, E. Conforto, C. Berziou, C. Savall, X. Feaugas, Grain size and grain-boundary effects on diffusion and trapping of hydrogen in pure nickel, Acta Materialia 60 (2012) 6814–6828.

[52] F. C. Frank, Symposium on the plastic deformation of crystalline solids, Pittsburgh, PA: Office of Naval Research, 1950.

[53] A. P. Sutton, R. W. Balluffi, Interfaces in crystalline materials, Oxford University Press, New York, NY, 1995.

[54] J. W. Cahn, Y. Mishin, A. Suzuki, Duality of dislocation content of grain boundaries, Philosophical Magazine 86 (2006) 3965–3980.

[55] J. W. Cahn, Y. Mishin, A. Suzuki, Coupling grain boundary motion to shear deformation, Acta Materialia 54 (2006) 4953–4975.

[56] S. Berbenni, B. Paliwal, M. Cherkaoui, A micromechanics-based model for shear-coupled grain boundary migration in bicrystals, International Journal of Plasticity 44 (2013) 68–94.

[57] P. R. M. vanBeers, V. G. Kouznetsova, M. G. D. Geers, M. A. Tschopp, D. L. McDowell, A multi scale model of grain boundary structure and energy: from atomistics to a continuum description, Acta Materialia 82 (2015) 513–529.

Table 1: Structural unit decomposition of symmetric tilt GBs about the [001] axis [45, 46]. a is the lattice parameter. In the decomposition bars denote one period of the boundary and the dot signifies that equivalent atoms in each half period are relatively displaced by $\frac{1}{2}$[0 0 1] along the tilt axis.

θ [°]	GB plane	$\mathbf{\Sigma}$	Structural decomposition of the period	Period vector $\mathbf{p}$
0.00	(1 1 0)	1	|A|	$\frac{a}{2}[\overline{1}\ 1\ 0]$
3.95	(15 14 0)	421	|AAAAAAAAAAAAAB.AAAAAAAAAAAAAB|	$a[\overline{14}\ 15\ 0]$
6.03	(10 9 0)	181	|AAAAAAAAB.AAAAAAAAB|	$a[\overline{9}\ 10\ 0]$
12.68	(5 4 0)	41	|AAAB.AAAB|	$a[\overline{4}\ 5\ 0]$
16.26	(4 3 0)	25	|AAB.AAB|	$a[\overline{3}\ 4\ 0]$
18.92	(7 5 0)	37	|AABAB|	$\frac{a}{2}[\overline{5}\ 7\ 0]$
20.02	(10 7 0)	149	|AABABAB.AABABAB|	$a[\overline{7}\ 10\ 0]$
22.62	(3 2 0)	13	|AB.AB|	$a[\overline{2}\ 3\ 0]$
25.06	(11 7 0)	85	|ABABABB|	$\frac{a}{2}[\overline{7}\ 11\ 0]$
28.07	(5 3 0)	17	|ABB|	$\frac{a}{2}[\overline{5}\ 5\ 0]$
30.51	(7 4 0)	65	|ABBB.ABBB|	$a[\overline{4}\ 7\ 0]$
33.40	(13 7 0)	109	|ABBBBBB|	$\frac{a}{2}[\overline{7}\ 13\ 0]$
35.30	(29 15 0)	533	|ABBBBBBBBBBBBBB|	$\frac{a}{2}[\overline{15}\ 29\ 0]$
36.87	(2 1 0)	5	|B.B|	$a[\overline{1}\ 2\ 0]$
39.60	(17 8 0)	353	|BBBBBBBC.BBBBBBBC|	$a[\overline{8}\ 17\ 0]$
42.08	(9 4 0)	97	|BBBC.BBBC|	$a[\overline{4}\ 9\ 0]$
43.60	(7 3 0)	29	|BBC|	$\frac{a}{2}[\overline{3}\ 7\ 0]$
46.40	(5 2 0)	29	|BC.BC|	$a[\overline{2}\ 5\ 0]$
48.89	(8 3 0)	73	|BCC.BCC|	$a[\overline{3}\ 8\ 0]$
51.11	(17 6 0)	325	|BCCCCC.BCCCCC|	$a[\overline{6}\ 17\ 0]$
53.13	(3 1 0)	5	|C|	$\frac{a}{2}[\overline{1}\ 3\ 0]$
54.95	(19 6 0)	397	|CCCCCCD.CCCCCCD|	$a[\overline{6}\ 19\ 0]$
56.60	(10 3 0)	109	|CCCD.CCCD|	$a[\overline{3}\ 10\ 0]$
58.11	(7 2 0)	53	|CCD.CCD|	$a[\overline{2}\ 7\ 0]$
61.93	(4 1 0)	17	|CD.CD|	$a[\overline{1}\ 4\ 0]$
64.94	(9 2 0)	85	|CDCDD.CDCDD|	$a[\overline{2}\ 9\ 0]$
67.38	(5 1 0)	13	|CDD|	$\frac{a}{2}[\overline{1}\ 5\ 0]$
71.08	(6 1 0)	37	|CDDD.CDDD|	$a[\overline{1}\ 6\ 0]$
73.74	(7 1 0)	25	|CDDDD|	$\frac{a}{2}[\overline{1}\ 7\ 0]$
78.58	(10 1 0)	101	|CDDDDDDD.CDDDDDDD|	$a[\overline{1}\ 10\ 0]$
82.37	(15 1 0)	113	|CDDDDDDDDDDDD|	$\frac{a}{2}[\overline{1}\ 15\ 0]$
90	(1 0 0)	1	|D|	$a[0\ \overline{1}\ 0]$

Table 2: Symmetric tilt GBs about the [001] axis disclination characteristics in Ni (lattice constant $a_{\mathrm{Ni}} = 0.3524$ nm)

θ [°]	Majority unit [Structural unit type]	Minority unit [Structural unit type]	Characteristic length d'_m of majority unit [nm]	Characteristic length d'_n of minority unit [nm]	Frank's vector magnitude ($\|\|\overrightarrow{\omega}\|\| = \omega$) [°]
3.95	13 [A]	1 [B]	0.2490	0.3778	±36.87
6.03	8 [A]	1 [B]	0.2488	0.3798	±36.87
12.68	3 [A]	1 [B]	0.2477	0.3852	±36.87
16.26	2 [A]	1 [B]	0.2467	0.3876	±36.87
18.92	3 [A]	2 [B]	0.2458	0.3892	±36.87
20.02	4 [A]	3 [B]	0.2454	0.3897	±36.87
22.62	1 [A]	1 [B]	0.2443	0.3909	±36.87
25.06	4 [B]	3 [A]	0.3919	0.2432	±36.87
28.07	2 [B]	1 [A]	0.3928	0.2417	±36.87
30.51	3 [B]	1 [A]	0.3933	0.2404	±36.87
33.40	6 [B]	1 [A]	0.3938	0.2387	±36.87
35.30	14 [B]	1 [A]	0.3949	0.2375	±36.87
36.87	1 [B]	0 [A]	-	-	±36.87
39.60	7 [B]	1 [C]	0.3939	0.5533	±16.26
42.08	3 [B]	1 [C]	0.3936	0.5546	±16.26
43.60	2 [B]	1 [C]	0.3933	0.5553	±16.26
46.40	1 [B]	1 [C]	0.3926	0.5562	±16.26
48.89	2 [C]	1 [B]	0.5568	0.3918	±16.26
51.11	5 [C]	1 [B]	0.5571	0.3910	±16.26
53.13	1 [C]	0 [B]	-	-	±16.26
54.95	6 [C]	1 [D]	0.5571	0.1680	±36.87
56.60	3 [C]	1 [D]	0.5569	0.1688	±36.87
58.11	2 [C]	1 [D]	0.5567	0.1694	±36.87
61.93	1 [C]	1 [D]	0.5556	0.1709	±36.87
64.94	3 [D]	2 [C]	0.1720	0.5542	±36.87
67.38	2 [D]	1 [C]	0.1728	0.5529	±36.87
71.08	3 [D]	1 [C]	0.1738	0.5504	±36.87
73.74	4 [D]	1 [C]	0.1744	0.5482	±36.87
78.58	7 [D]	1 [C]	0.1753	0.5435	±36.87
82.37	12 [D]	1 [C]	0.1758	0.5391	±36.87

Table 3: Materials parameters for H in nickel.

Property	Symbol	Value	Unit	Ref.
Shear modulus	μ	76	GPa	
Poisson's ratio	ν	0.31		
Lattice constant	a	0.3524	nm	
Atomic volume	Ω	10.94	Å^3	
Solute relaxation volume	ΔV	0.13Ω	Å^3	[50]